IEEE Access
Multidisciplinary ⋮ Rapid Review ⋮ Open Access Journal

Received 10 July 2023, accepted 8 August 2023, date of publication 14 August 2023, date of current version 18 August 2023.

Digital Object Identifier 10.1109/ACCESS.2023.3304751

RESEARCH ARTICLE

Precise Automation of Rotary Flexible Link Manipulator Using Hybrid Input Shaping With Single State Feedback Fuzzy Logic and Sliding Mode Controllers

AHMAD BALA ALHASSAN[1], RATCHATIN CHANCHAROEN[1,2], BASHIR BALA MUHAMMAD[1], AND GRIDSADA PHANOMCHOENG[1,2,3]

[1]Department of Mechanical Engineering, Chulalongkorn University, Bangkok 10330, Thailand
[2]Micro/Nano Electromechanical Integrated Device Research Unit, Faculty of Engineering, Chulalongkorn University, Bangkok 10330, Thailand
[3]Applied Medical Virology Research Unit, Chulalongkorn University, Bangkok 10330, Thailand

Corresponding author: Gridsada Phanomchoeng (gridsada.phanomchoeng@gmail.com)

This work was supported by the Ratchadapisek Somphot Fund for Postdoctoral Fellowship through the Graduate School, Chulalongkorn University, Bangkok, Thailand.

ABSTRACT Flexible link manipulators (FLM) are widely preferred in applications that require faster operation, high maneuverability, and less energy consumption. However, their flexibility is associated with undesired vibrations, making accurate positioning challenging. As most of the existing controllers are model-based, their performances are affected by uncertainties and often require the feedback of all the states. This makes such control challenging and expensive. Interestingly, despite its poor position tracking, the input shaping control (ISC) proved to be effective in oscillation suppression of flexible structures. In this paper, precise automation of the FLM is presented by hybridizing an improved input shaping control (iISC) with a model-free fuzzy logic control (FLC), and the model-based sliding mode control (SMC). The single feedback FLC, and SMC were designed for the position control while the iISC provided the tip deflection control. Three parameters of the FLM, namely, the length, mass, and spring stiffness of the link were used to assess the sensitivity of the controllers. With the maximum velocity of 94 deg/s and the maximum r.m.s of 0.33 deg, ISC+FLC has increased the velocity of the iISC by at least 77% and improved the poor oscillation suppression of the FLC by at least 64%. Thus, the analysis demonstrated that the iISC+FLC could provide precise automation of the FLM by measuring the output of only one state (position), making it cost-effective and reduces the complexity and computation time of the full-state feedback controllers.

INDEX TERMS Dynamic modelling, flexible link manipulator, position tracking, sensitivity analysis, tip deflection, vibration suppression.

I. INTRODUCTION

With the advancements in robotics, industrial companies have heavily invested in research and development of flexible robotic manipulators that offer improved productivity and help to meet the increasing demand of manufacturing [1]. Traditionally, heavy rigid manipulators were deployed in the assembly lines for many tasks including pick and place, welding, and track-tracking [2]. However, these rigid manipulators require bulky drives, have high link mass, have limited speed, and can consume a lot of energy [3], [4]. Interestingly, flexible link manipulators were introduced as an alternative to rigid link manipulators. Due to their light-weight and flexibility, the FLMs consume less energy, need smaller actuators, and can function at high speed with low inertia. Furthermore, the FLMs are generally cost-effective, have

The associate editor coordinating the review of this manuscript and approving it for publication was Ming Xu.

a higher payload-to-link weight ratio, and possess a high degree of maneuverability, among others [5]. The potential application of FLM for collaborative robotics for an increase payload-to-mass ratio was investigated extensively in [6]. Thus, the application of FLMs can be extended to the food industry for packaging and palletizing, construction, aerospace, nuclear fusion, and the health industry for robotic surgeries [7], [8], [9].

Nonetheless, the flexibility of the FLM makes it prone to undesirable vibrations, making accurate positioning challenging [10]. Therefore, it is very crucial to provide efficient and effective control strategies to suppress the induced vibrations for optimal operations of flexible manipulator systems. Remarkably, there have been numerous studies for the dynamic modeling and control of the FLMs, ranging from classical control to intelligent control algorithms as comprehensively surveyed in [11] and [12]. For instance, Shao et al. [13] presented the dynamic modeling of FLM using finite element analysis. The derived model was reduced while maintaining its precision using an iterative reduction system which allows easy design and implementation of LQR control. Altiner et al. al [14] modelled the single link FM using spatial differential equations and designed a control that compensates the effects of unmodeled dynamics. Also, to reduce the complexity of control implementation, and the need for fewer actuators/sensors, a dynamic trajectory planning and fuzzy self-tuning for residual vibration suppression of FLM was presented in [15]. In [16], a disturbance-observer-based active vibration control of a FLM was presented. The study modelled the FLM as an Euler-Bernoulli beam taking into account the spatially infinite dimensional disturbance.

Fareh et al. [17] designed a sliding mode control based robust disturbance rejection system. The work estimate both internal and external disturbances which were compensated in real-time. One of the limitations of the SMC is the inherent chattering which if persistent could lead to motor burnt-out. Thus, Cheng et al. [18] presented a chattering suppression technique for the flexible joint manipulator. As most of the existing works focused on the FLM, Zhu et al. [19] proposed a composite controller for a flexible link and joint under disturbance and uncertainties. The composite material consists of adaptive-gain super twisting SMC for the position tracking and the adaptive dynamic programming for the boundary layer stabilization. Also, Belherazem and Chenafa [20] presented a passivity based adaptive control for the FLM. The control system combined the passivity based approach and the adaptive mechanism which guarantee online parameter estimation under external disturbance. As the application of FLM can be extended to ocean exploration, Huang et al. [21] presented the mathematical modeling and control of a two-link underwater FLM.

In [22], the velocity profile was used to reduce the end-point transient and residual vibrations of FLM during high speed operations. In some applications, the hybrid rigid-flexible manipulators were introduced to utilize the advantages of the two systems. In [23], the mathematical modeling and position tracking of a mobile rigid-flexible manipulator was presented. The study established an adaptive fault-tolerant control in the event of actuator failure and ensured the displacement of the vehicle is within the allowable constraints. Other research includes the performance analysis of FLM gripper with magnetorheological grease [24], surface control of multi-link flexible joint manipulators [25], design and analysis of pneumatic flexible manipulators [26].

Furthermore, most of the research on FLM uses physical laws to derive the dynamic equations of the FLM for analysis and control. However, model uncertainties are generally associated with those methods which could affect the performance of the controller in practical applications. Bastos [27] proposed a non-inherent parameter estimation for the equivalent dynamic equations of the FLM with parallel and serial kinematics. Also, Lara-Molina and Gonçalves et al. [28] presented a reliability based optimization approach using stochastic finite element dynamic modelling of the FLM. The study achieved optimal design of the FLM whereby the actuator power, manipulator mass, and overall reliability of the FLM were optimized. As highlighted above, there has been a lot of improvement in the design of controllers for position tracking and vibration suppression of FLM over the years. However, the feedback controllers require much sensors and complex computation. In addition, the model-based controllers which are the most widely research controllers are often affected by the model-errors and uncertainties or external disturbances.

In this study, an approach for precise automation of rotary FLM using the feed-forward ISC and feedback FLC, and SMC is presented. The advantage of iISC for the oscillation suppression and the position control capability of the FLC, and SMC were utilized. One of the contributions of the work is that the conventional ISC was enhanced (iISC) by smoothing the reference signal of the ISC using first order filter. This reduces the chattering issues of the ISC and also minimizes the unnecessary delay associated with the ISC. Secondly, the iISC was hybridized with the FLC, and SMC, respectively for the accurate position and tip deflection control of the FLM. The SMC was designed based on the dynamic model of the FLM while the FLC is non-model based. The performances of the two hybrid configuration, namely iISC+FLC, and iISC+SMC were extensively analyzed including sensitivity analysis to model parameter changes.

The paper is divided into five main parts. The description and the mathematical modelling of the FLM system was presented in part 2. The control theories were presented in section III. The simulation result and analysis were presented in section four. Finally, the conclusion of the paper is highlighted in section five.

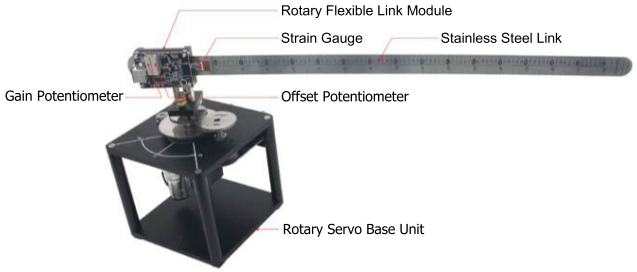

FIGURE 1. A typical Rotary flexible link manipulator where the electronic sensing unit attached to flexible link is mounted on a rotary servo base unit. The link can be rotated clockwise or counter clockwise using the servo motor of the robot. The deflection of the link is measured by strain gage which outputs analogue signal proportional to the link deflection [29].

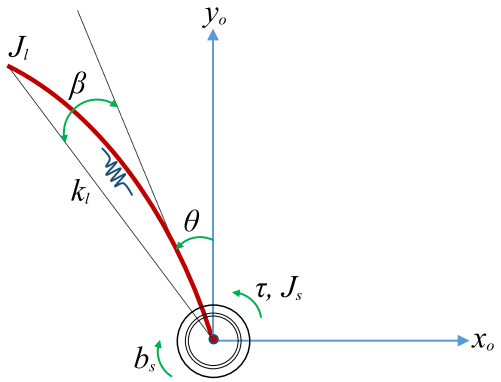

FIGURE 2. The schematics of the flexible link which is represented as a linear spring with a stiffness of k_l.

II. SYSTEM DESCRIPTION AND MODELLING

A. THE ROTARY FLEXIBLE LINK SYSTEM

The study of rotary FLM provides an excellent opportunity to explore the analysis and control of vibration and resonance in large, light structures that possess flexibilities. The analysis also proves beneficial for creating models of flexible links in robots or spacecraft. The typical laboratory flexible link manipulator is shown in Fig. 1. The system which is adopted by the Quanser Inc. has been used by many researchers around the world for dynamic analysis and implementation of numerous control theories. As illustrated, the rotary FLM module contains a flexible link made of stainless steel and equipped with a strain gauge that can sense the deviation of the link's tip. The electronic circuit board consisting of strain gauge, potentiometers and the link module is attached to the fixed end of the flexible link and mounted on the SRV02 servo system. When attached to the rotary servo base unit, the module rotates the flexible link in a horizontal plane.

B. THE DYNAMIC MODELLING OF THE FLM

Dynamic model is essential for the design and analysis of any control scheme. The models allows for an in-depth analysis of the system before applying the control on a physical system. Here, the rotary FLM is presented by considering the link to be linear spring. The detail modelling of the FLM was presented in [29]. The main objective of the control system is move the link to a certain position precisely without oscillation or deflection of the link. The automation of the FLM depends on the rotation of the motor. Thus, the servo generates a torque, τ which rotates the flexible link to an angle, θ as shown in Fig. 2. However, since the link is flexible, it will deflect from the reference θ with the deflection angle, β. The link has a mass of m_l, a length of L_l, and a moment of inertia about its centre of mass, J_l. To model the flexible link, the link can be represented as a linear spring with a stiffness of k_l. As the servo rotates, its rotation will be opposed by the viscous friction b_s.

Therefore, to derive the dynamic equations of the FLM, the Lagrangian equations of Eq. (1), and Eq. (2) were utilized, where Q_i is the combined non-conservative forces, m_i is the mass of the ith variable, and q_i is the ith coordinate of an independent point. The overall Kinetic, T energy and the potential energy, U of the hub and the link can be represented in Eq. (3) and Eq. (4), respectively.

$$\frac{d}{dt}\left(\frac{dT}{d\dot{q}_i}\right) - \frac{dT}{dq_i} + \frac{dU}{dq_i} = Q_i; \quad i = 1, 2, 3 \ldots n \tag{1}$$

$$T = \sum_{i=1}^{n} \frac{1}{2} m_i \dot{q}_i^2; \quad U = \sum_{i=1}^{n} (m_i g h_i) \tag{2}$$

$$T = \frac{1}{2} J_s \dot{\theta}^2(t) + \frac{1}{2} J_l (\dot{\theta}^2(t) + \dot{\beta}^2(t) + 2\dot{\theta}\dot{\beta}(t)) \tag{3}$$

$$U = \frac{1}{2} k_l \beta^2(t) \tag{4}$$

After solving for Eq. (1) using the expression of Eq. (3) and Eq. (4), the complete dynamic equations of the rotary single link FLM can be represented in Eq. (5) and Eq. (6):

$$\ddot{\theta}(t) = \frac{\tau(t)}{J_s} - \frac{b_s}{J_s}\dot{\theta}(t) + \frac{k_l}{J_s}\beta(t) \tag{5}$$

$$\ddot{\beta}(t) = -\frac{\tau(t)}{J_s} + \frac{b_s}{J_s}\dot{\theta}(t) + k_l\left(\frac{1}{J_s} + \frac{1}{J_l}\right)\beta(t) \tag{6}$$

Furthermore, as illustrated in the schematics of Fig.2, the torque that rotates the FLM is created by the motor attached to the hub.Thus, to integrate the motor parameters in the FLM's equations of Eq. (5), and Eq. (6), the relationship between the reference voltage, $V_{ref}(t)$, and motor torque, $\tau(t)$ of Eq. (7) was used, where R_m is the motor armature resistance, η_m is the motor efficiency, η_g is the gear box efficiency, k_g is the gear ratio, k_m is the motor back e.m.f, and k_t is the motor torque constant. The values of these parameters are provided by the Quanser FLM datasheet as shown in Table 1.

$$\tau(t) = \frac{\eta_g k_g \eta_m k_t (V_{ref}(t) - k_g k_m \dot{\theta}(t)) k_m}{R_m} \tag{7}$$

Finally, after substituting the motor dynamics of Eq. (7) in the dynamic model of Eq. (5) and Eq. (6), the state space representation of the complete FLM can be represented according to Eq. (8) in Eq. (9), where y_{op} is the system's output including the FLM's position, linear velocity, and tip

TABLE 1. Dimension and parameters of the rotary FLM [29].

Parameter	Symbol	Value
Tip deflection angle	β	-
Link angular position	θ	-
Motor Torque	τ	-
viscous friction	b_s	0.04
Link linear spring stiffness	k_l	1.3 Nm
Length of the link	L_l	0.419 m
Mass of the link	m_l	0.065 Kg
Link moment of inertia	J_l	0.0038
Hub moment of inertia	J_s	0.00208
Motor armature resistance	R_m	2.6 Ω
Motor efficiency	η_m	69%
Gear box efficiency	η_g	90%
Gear ratio	k_g	70
Motor back e.m.f	k_m	0.00768 V/rad/s
Motor torque constant	k_t	0.00768 Nm/A

deflection. z(t) is the state vector, u(t) is the input vector, *A*, *B*, and *C*, are the constant system matrices.

$$\dot{z}(t) = Az + Bu(t);\ y_{op} = Cz(t) \tag{8}$$

$$\begin{bmatrix} \dot{\theta}(t) \\ \ddot{\theta}(t) \\ \dot{\beta}(t) \\ \ddot{\beta}(t) \end{bmatrix} = \begin{bmatrix} 0 & 1 & 0 & 0 \\ 0 & -\left(\frac{b_s}{J_s} + \frac{\eta_g k_g \eta_m k_t k_g k_m}{J_s R_m}\right) & \frac{k_l}{J_s} & 0 \\ 0 & 0 & 0 & 1 \\ 0 & \left(\frac{b_s}{J_s} + \frac{\eta_g k_g \eta_m k_t k_g k_m}{J_s R_m}\right) & -\left(\frac{k_l}{J_s} + \frac{k_l}{J_l}\right) & 0 \end{bmatrix}$$

$$\times \begin{bmatrix} \theta(t) \\ \dot{\theta}(t) \\ \beta(t) \\ \dot{\beta}(t) \end{bmatrix} + \begin{bmatrix} 0 \\ \frac{\eta_g k_g \eta_m k_t}{J_s R_m} \\ 0 \\ -\frac{\eta_g k_g \eta_m k_t}{J_s R_m} \end{bmatrix} V_{ref}(t);\ y_{op}$$

$$= \begin{bmatrix} 1 & 0 & 0 & 0 \\ 0 & 1 & 0 & 0 \\ 0 & 0 & 1 & 0 \end{bmatrix} \begin{bmatrix} \theta(t) \\ \dot{\theta}(t) \\ \beta(t) \\ \dot{\beta}(t) \end{bmatrix} \tag{9}$$

III. CONTROL DESIGN

This section provides a comprehensive analysis of control schemes for the rotary RFLM's position, speed, and tip angle deflection control. Three controllers namely, ISC, FLC, and SMC were investigated for the possible hybrid configuration. However, it is necessary to check if the system can be controlled before proceeding with the design. This

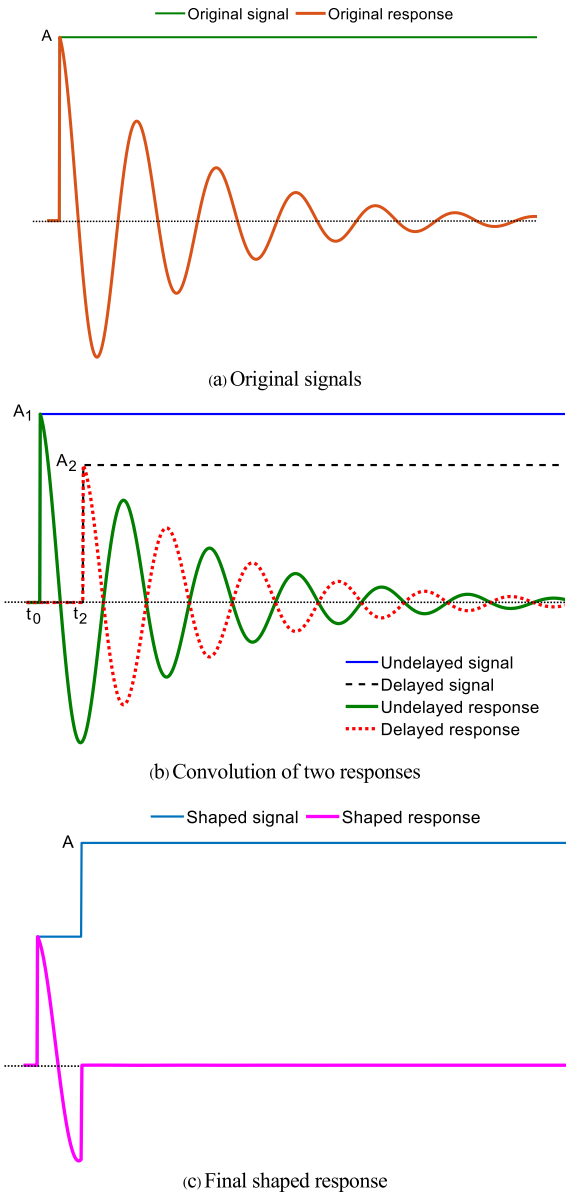

FIGURE 3. The graphical process of ISC: (a) The original signal was applied to the system resulting in the oscillation response of peak amplitude, A; (b) Part of the signal is applied to the system without any delay, and the other part is delayed for time, t_2 such that $A_1+A_2 = A$; (c) The convolution of the two responses canceled the oscillation.

can be done by calculating the controllability, G_c, of the system using the controllability matrix of Eq. (10). The controllability test proved that the system is controllable, allowing the design of the controllers.

$$G_c = \left[B\ AB\ A^2B\ A^3B \right];\ |G_c| \neq 0 \tag{10}$$

A. INPUT SHAPING CONTROL ISC

Input shaping or command shaping control is an effective control method that reduces oscillation of flexible systems without requiring the need of feedback or physical system redesign. The process of input shaping or time delay

containing two impulses is illustrated in Fig. 3. As shown, part of the signal is delayed and then convolved with the un-delayed signal to cancel the effect of the induced oscillations. However, the choice of appropriate shaper's amplitude and their respective time delays must be determine effectively, otherwise, the oscillation will be exacerbated.

Thus, generally these parameters were obtained using the general representation of the second-order underdamped system of Eq. (11), as shown at the bottom of the next page, or its equivalent time domain of Eq. (12), as shown at the bottom of the next page, where $A_i$is the ith impulse amplitude, t_i is the ith impulse, ω is the natural frequency, and ζ is the damping ratio.As illustrated, the ISC is designed using the estimated ω and ζ.

The non-dimensional oscillation's magnitude can be calculated by dividing Eq. (12) with the results of a single impulse of magnitude one at rest, leading to the residual oscillation of Eq. (13), as shown at the bottom of the next page. This is the oscillations produced by an impulse sequence of an under-damped system ($\zeta < 0$). The amount of the allowable oscillation can be set to Eq. (13) based on the selected constraints. If zero oscillation is needed, then R_1 and R_2 of Eq. (13) should be set to zero also known as the zero oscillation constraint.Also, to maintain the behavior of the rigid body motion of the unshaped signal, the total amplitude of the shapers' should be one (1), also known as the summation constraint as in Eq. (14), as shown at the bottom of the next page.

Also, the undesirable response delay can be avoided by applying the first impulse at $t_1 = 0$. Nonetheless, the ZO shaper is not robustness to model variations**.** Thus, the performance can be enhanced by taking the derivatives of R_1 and R_2 and then equate to zero. Here, a small change in oscillation in relative to the model variations will be ensured**.** In this study, the second-order shaper shown in Eq. (15) is considered**.** In addition, to determine the design parameters, the logarithmic decrement method was utilized**.** Details design and robustness analysis of these shapers are described in our previous analysis [30].

$$\begin{bmatrix} A_i \\ t_i \end{bmatrix} = \begin{bmatrix} \frac{1}{(1+k)^3} & \frac{3k}{(1+k)^3} & \frac{3k^2}{(1+k)^3} & \frac{k^3}{(1+k)^3} \\ 0 & \tau_d & 2\tau_d & 3\tau_d \end{bmatrix}$$
$$; \tau_d = \frac{\pi}{\omega\sqrt{(1-\zeta^2)}}; k = e^{\frac{-\pi\zeta}{\sqrt{(1-\zeta^2)}}} \quad (15)$$

B. SLIDING MODE CONTROL SMC

The SMC is designed to achieve continuous control in a sliding mode platform, such that the output response tracks the reference trajectory accurately. The controller has demonstrated good trajectory tracking and regulator action even in the presence of external disturbances or parameter variations [31]. The primary objective is position tracking since the tip deflection is suppressed by the iISC. Figure 4 [32] shows the typical process of SMC, where the sliding surface, s forced the system states to follow the desired

TABLE 2. Membership table for the I/O rules.

		Position Error						
		NB	NM	NS	ZE	PS	PM	PB
Change of Error	NB	NB	NB	NB	NB	NM	NS	ZE
	NM	NB	NB	NB	NM	NS	ZE	PS
	NS	NB	NB	NM	NS	ZE	PS	PM
	ZE	NB	NM	NS	ZE	PS	PM	PB
	PS	NM	NS	ZE	PS	PM	PB	PB
	PM	NS	ZE	PS	PM	PB	PB	PB
	PB	ZE	PS	PM	PB	PB	PB	PB

trajectory, where a is the positive constant, θ_d is the desired trajectory, and e is the tracking error. The sliding surface, s that drives the states to their origin is defined in Eq. (16).

$$s = ae(t) + \dot{e}(t); e = \theta_d(t) - \theta(t)\ ; a > 0 \quad (16)$$

When the sliding surface is driven to zero (s = 0), the desired response is achieved and the tracking error will converge to zero. Secondly, the reaching law of Eq. (17) which boost the states to reach the sliding surface as quickly as possible is selected. This function is selected due to its advantage of non-chattering switching effects unlike the usual signum (sign) function. The positive constant ρ, and r determined the speed and convergence of the tracking error.

$$\dot{s} = -\rho(s)^r; \rho > 0, 0 < r \leq 1 \quad (17)$$

Here, only the link position, θ is controlled using the SMC while the angle, β was controlled by the iISC. Thus, taking the derivative of the sliding surface yields the reaching surface of Eq. (18). Subsequently, substituting the relevant parameters of the system in Eq. (9) into Eq. (18) gives the corresponding reaching surface in Eq. (19).

$$\dot{s} = a\dot{e}(t) + \ddot{e}(t); a > 0 \quad (18)$$
$$\dot{s} = -(a + A_{22})\dot{\theta}(t) - A_{23}\beta(t) - B_{21}u(t) \quad (19)$$

Finally, the control law, u(t) of Eq. (20) is derived by equating the reaching law of Eq. (17) and Eq. (19).

$$u(t) = \frac{1}{B_{21}}\{-(a + A_{22})\dot{\theta}(t) - A_{23}\beta(t) + \rho\left((\theta_d(t) - \theta(t))\, a - \dot{\theta}(t)\right)^r\} \quad (20)$$

where the parameters A_{22}, A_{23} are the elements of the system matrix while B_{21} is the element of the input matrix of Eq. (9). The values of the control parameters were selected as tabulated in Table 3.

C. FUZZY LOGIC CONTROL FLC

As earlier stated, the ISC provides effective oscillation control but it is affected by the variations of system parameters.Other controllers like the SFB require all the states to be feedback (expensive) and it is sensitive to change of system parameters as well.Thus, a non-model dependent control like the FLC will be a good alternative to

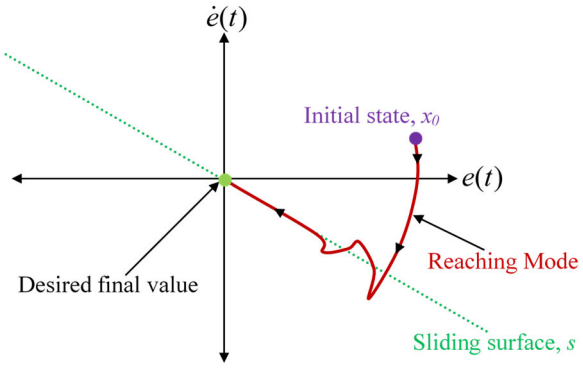

FIGURE 4. The process of sliding mode control (SMC).

TABLE 3. Control parameters for the analysis.

Controller	Parameters
iISC	$\tau_d = 0.1550$; k = 0.3610
SMC	a = 10 ; ρ = 60 ; r = 0.4
iISC+SMC	a = 2.12 ; ρ = 55 ; r = 1
iISC+FLC	$u = \pm 360$; error = ± 90 ; change of error = $\pm 4.5E{+}15$

the aforementioned controllers.To tune the input and output variables of the FLC, the control signal characteristics of the SFB was used.Using this approach, control signal of the SFB for each state is the optimal value as they were chosen for the model parameters.Thus, the FLC uses the advantages of the pole placement-based SFB to select the ranges of its input and output variables.

Unlike the SFB that requires full state, the FLC in this design only measure one state (position). Therefore, it is cheaper, and doesn't require the system model for the design.The ranges of the error, change of error and output control were chosen as ±90, ±4.5e15, and ±360, respectively as shown in the membership function plot of Fig.5.The membership table for the FLC is illustrated in Table 2, which covers the whole operating condition of the FLM.The membership functions of the Mandani inference system were chosen to be Gaussian for the input and output variables.Also, the centroid defuzzification method was chosen while other parameters take the default settings.

D. HYBRID iISCFLC, AND iISCSMC SCHEMES

In this section, the hybrid iISC+FLC, and iISC+SMC techniques are discussed. As stated earlier, the iISC in a feedforward configuration has proved to effectively suppress the oscillation of the FLM. The ISC uses time delays at a specified time to cancel the effect of vibration [33] To compute the control gains of the iISC for the FLM tip deflection control, the logarithmic decrement was employed. The natural frequency of 21.3075 Hz and damping ratio of 0.3085 of the FLM were obtained. These parameters were then inserted in the ISC of Eq. (15) to compute the desired amplitudes and time delay. Then, the iISC was achieved by adding a filter to the ISC to shape the resulting signal chattering, as illustrated in Eq. (21).

$$\begin{bmatrix} A_i \\ t_i \end{bmatrix} = \begin{bmatrix} 0.3966 & 0.4296 & 0.1551 & 0.0187 \\ 0 & 0.1550 & 0.3100 & 0.4650 \end{bmatrix} \cdot \left(\frac{15}{s+15} \right) \tag{21}$$

On the one hand, the FLC, and SMC were used as the feedback control for the position tracking. For precise automation of the FLM, design criteria for the overshoot, and settling time were set to 0.5% and 1 seconds, respectively. Therefore, after performing the required calculations, the controllers were applied in the Simulink configuration of Fig. 6. As shown, iISC is connected at the reference point for shaping the signal to the FLC, and in-front of the SMC. The configuration is best implementation structure of the controllers after analyzing their performance at the potential positions**.** To investigate the performance of the SMC, the

$$G(s) = \frac{\omega^2}{s^2 + 2\zeta\omega s + \omega^2} \tag{11}$$

$$A = \frac{\omega}{\sqrt{(1-\zeta^2)}} e^{-\zeta\omega t_i} \sqrt{\left(\sum_{i=1}^{n} A_i e^{\zeta\omega t_i} \cos\left(\omega t_i \sqrt{(1-\zeta^2)} \right) \right)^2 + \left(\sum_{i=1}^{n} A_i e^{\zeta\omega t_i} \sin\left(\omega t_i \sqrt{(1-\zeta^2)} \right) \right)^2} \tag{12}$$

$$V(\omega, \zeta) = e^{\zeta\omega t_i} \sqrt{\left(\underbrace{\sum_{i=1}^{n} A_i e^{\zeta\omega t_i} \cos\left(\omega t_i \sqrt{(1-\zeta^2)} \right)}_{R_1} \right)^2 + \left(\underbrace{\sum_{i=1}^{n} A_i e^{\zeta\omega t_i} \sin\left(\omega t_i \sqrt{(1-\zeta^2)} \right)}_{R_2} \right)^2} \tag{13}$$

$$\sum_{i=1}^{n} A_i = 1 \tag{14}$$

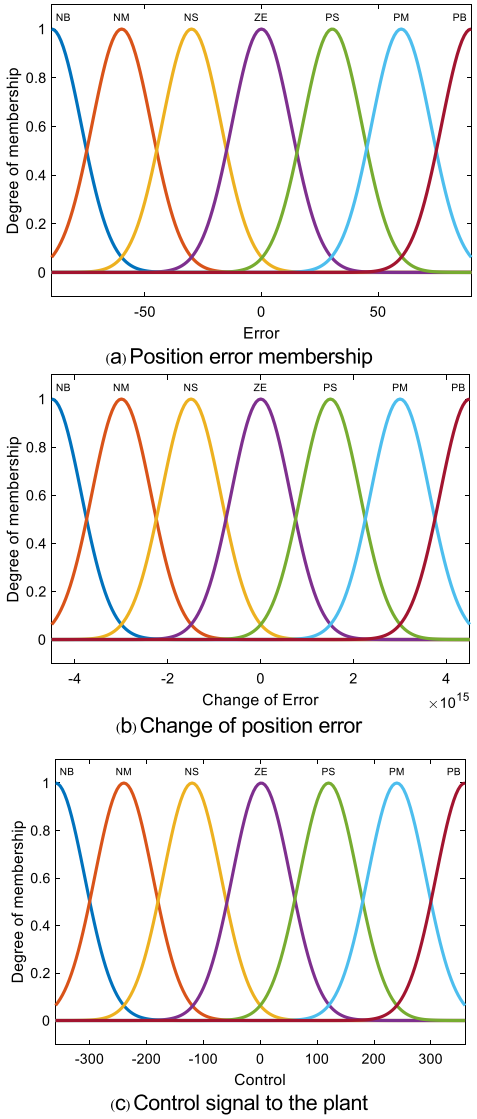

FIGURE 5. The FLC membership plot for the two-input one-output FLC.

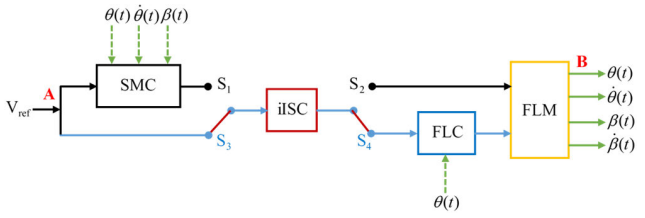

FIGURE 6. The hybrid configuration of the iISC with the single state feedback FLC, and three states feedback SMC.

switches S_1 and S_2 were turned ON whereas the iISC+FLC was analyze by switching S_3 and S_4.

In sum, the hybrid set-up uses the benefits of the iISC, and FLC and SMC for the precise automation of the FLM**.** The key importance of the iISC+FLC is that it only uses one feedback signal (position) as compared to the iISC+SMC that uses three feedback signals (position, velocity, and tip

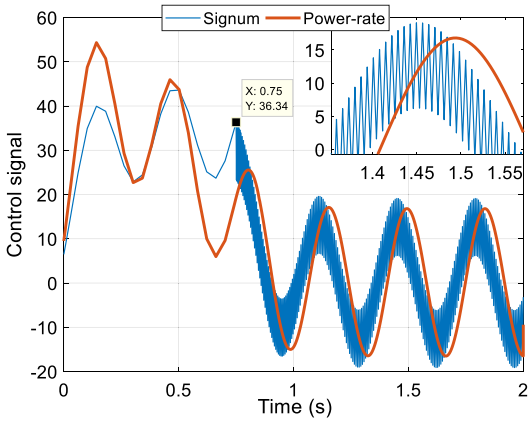

FIGURE 7. The control input u(t) showing the smooth signal from power-rate as compared to the signum with a lot of chattering.

deflection). The controllers would be assess based on time response specifications, namely, settling time (braking), and tip deflection suppression. The parameters for the control performance analysis are presented in Table 3.

E. STABILITY ANALYSIS

Stability analysis is a standard requirement for any control design to ensure that the control system does not loss its stability within a certain operating bound.One of the widely accepted method for the stability analysis is the Lyapunov approach such that the stability of the closed-loop system can be guaranteed by adopting the Lyapunov rules [34].

Remark 1: One of the requirement is that sliding mode should start at a finite time, t > 0, irrespective of the initial condition of the states $x(0)$. Thus, the trajectory is always moving towards s = 0 when s is not yet at zero.This is called the reaching condition as expressed in Eq. (22). However, s becomes slower when it approaches zero which delayed the convergence.

$$\frac{d}{dt}s^2 < 0 \Rightarrow s\dot{s} < 0 \tag{22}$$

Therefore, the signum is proven to have chattering effects due to abrupt switching near zero. This phenomenon not only generate noise but also effects the actuator's operation. Thus, one of the chattering suppression approach is the use of smoother power-rate reaching law [35], [36], [37]. In this approach the reaching law of Eq. (17) was adopted. Figure 7 shows the comparison between the signum and the power-rate reaching law for the system. As shown, signum has a lot of chattering as the state approaches zero unlike the smooth signal of the chosen power-rate function.

Theorem 1: The Lyapunov theorem was adopted for the final stability assessment.The Lyapunov candidate of Eq. (23) is selected.The theorem states that the derivative of the Lyapunov function of Eq. (24) must be negative for the

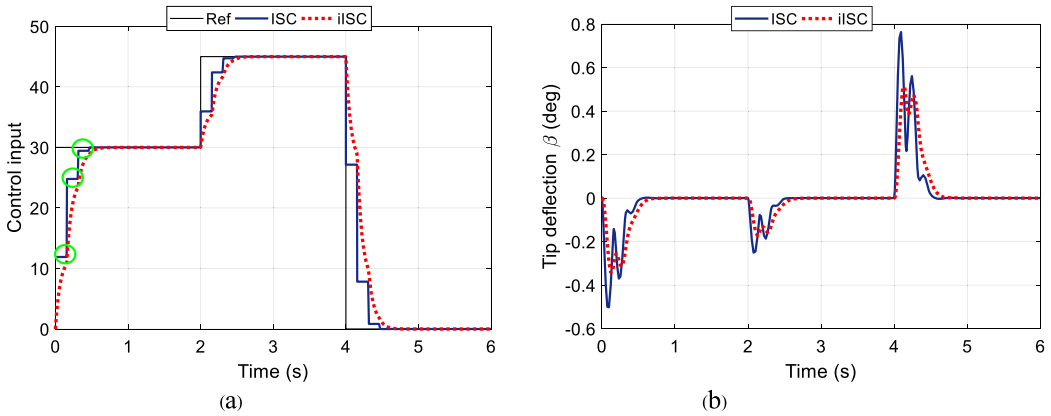

FIGURE 8. Performance comparison for ISC and iISC: (a) Reference signal showing the improved ISC with reduced chattering; (b) Tip deflection showing the improved oscillation suppression.

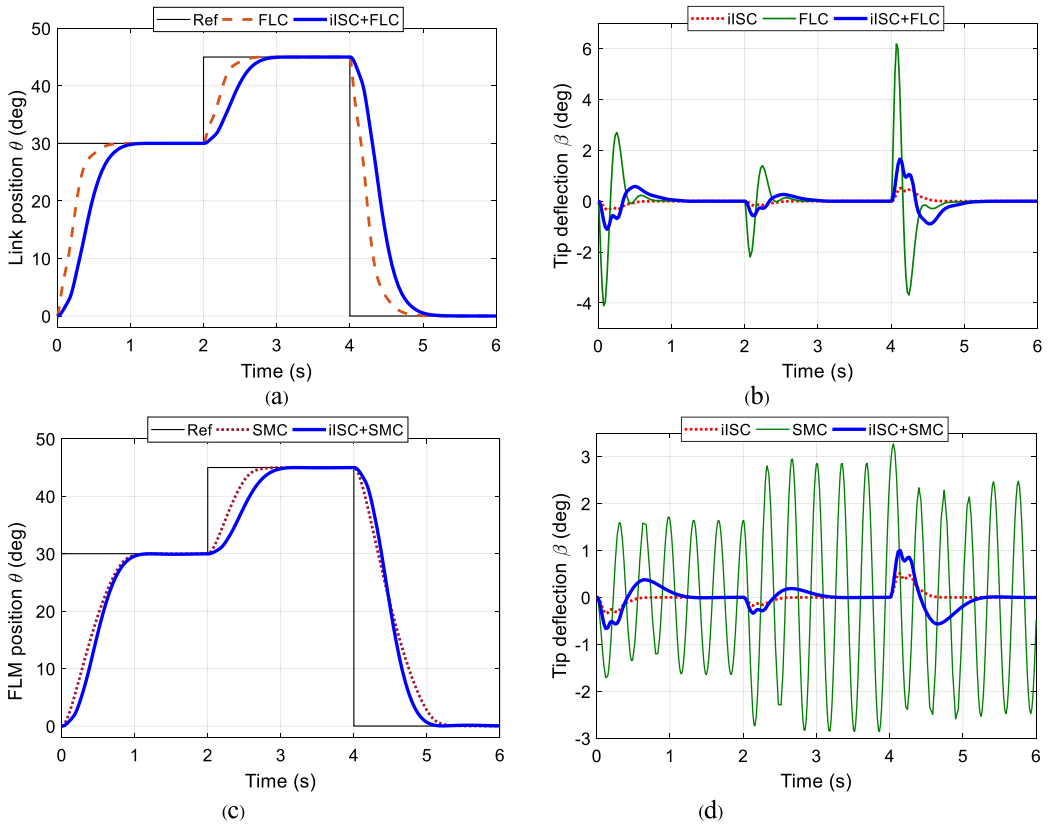

FIGURE 9. Performance comparison of FLC, SMC, iISC+FLC, and iISC+SMC: (a) Position control of FLC; (b) Tip deflection suppression of the FLC; (c) Position tracking of SMC; (d) Tip deflection suppression of the SMC.

system to be asymptotically stable.

$$V_{LF}(s,t) = \frac{1}{2}s^2 \tag{23}$$

$$\dot{V}_{LF} = s\dot{s} = s\left(-\rho(s)^r\right);\ \rho > 0, 0 < r \leq 1 \tag{24}$$

For the switching function to be strictly asymptotically stable (Eq. (24) < 0), the following two conditions must be satisfied. For the combined control, the second condition holds for r = 1 as shown in Table 3.

$$\dot{V}_{LF} < 0 : \begin{cases} -\rho\left|s^{(r+1)}\right| & if\ \rho > 0, 0 < r < 1 \\ -\rho\left(s^2\right) & if\ \rho > 0, r = 1 \end{cases} \tag{25}$$

IV. RESULTS AND DISCUSSION

Herein, the results of the control approaches were studied using the mathematical model of the rotary FLM of Eq.(9) in Matlab simulation environment.The system is given a

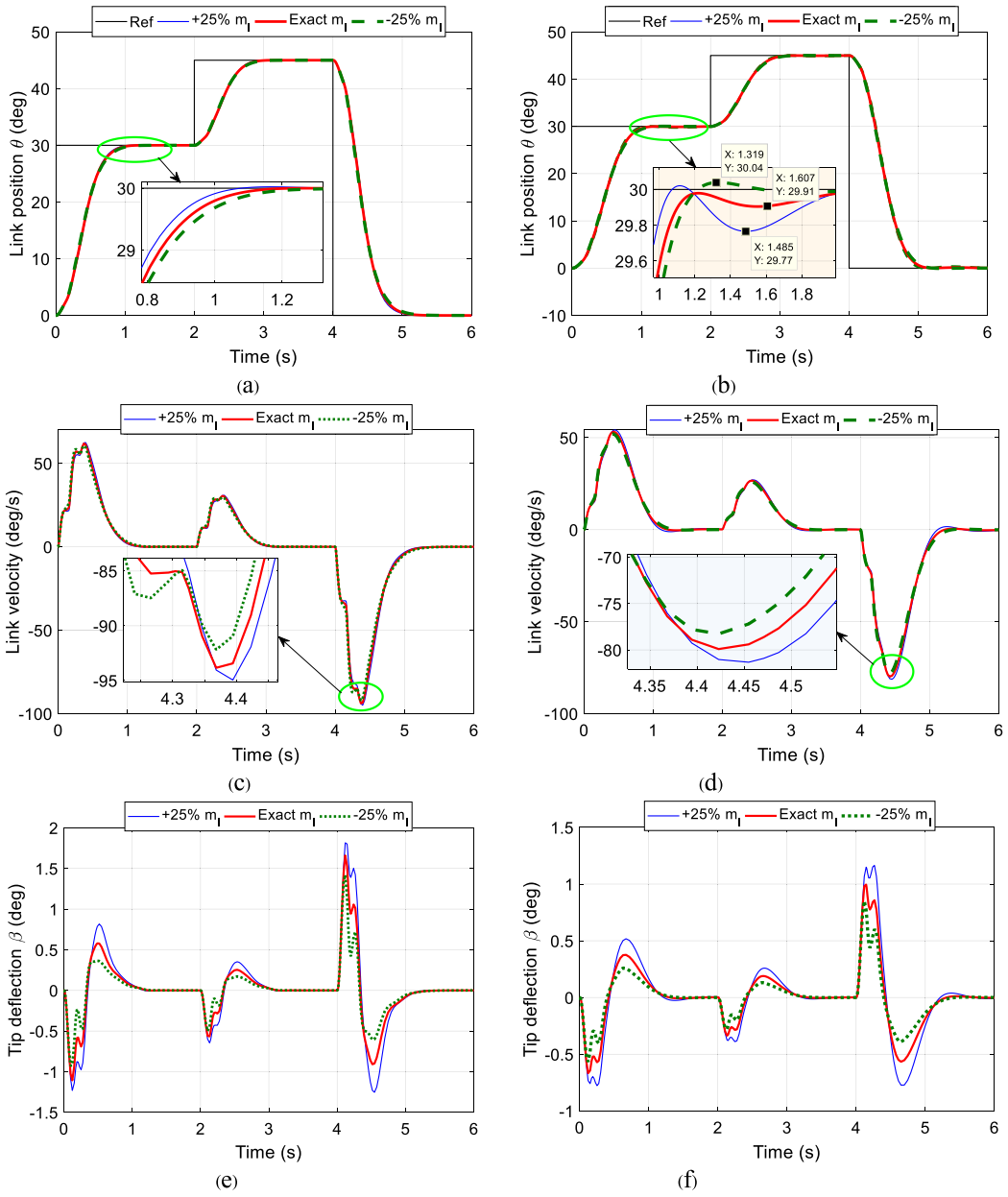

FIGURE 10. Sensitivity to changes of link mass: (a) Position control of iISC+FLC; (b) Position control of iISC+SMC; (c) Link velocity for iISC+FLC; (d) Link velocity for iISC+SMC; (e) Tip deflection for iISC+FLC; (f) Tip deflection for iISC+SMC.

reference trajectory such that it rotates to 30 degree for one second, stays there for another one second and then move to 45 degrees before finally returning to the initial position of zero degree.This will allow the behavior of the system to be fully analyzed in terms of response time specification and oscillations characteristics.The position tracking is analyzed in terms of time response specifications particularly the rise time, overshoot and settling time whereas the level of tip deflection suppression is analyzed by calculating the r.m.s of the response.The smaller the value of the r.m.s, the higher the amount of deflection reduction.

A. PERFORMANCE COMPARISON OF ISC, FLC, SMC, iISCFLC, AND iISCSMC

To compare the performance of three designed controllers namely, ISC, FLM and SMC, the Simulink model in Fig.6 was used.Firstly, the ISC, FLC, and SMC were implemented separately and then hybridized with the improved ISC (iISC). The iISC was installed at the feedforward scheme of the FLC and SMC, respectively.The results for all the configurations were studied.Figure 8a shows the shaped signal of the ISC and iISC, whereby the chattering effect (circled) of the ISC is clearly eliminated using filter described in Eq. (21). The improvement of the iISC can be further visualized in

Fig.8b, where the maximum tip deflection of the FLM was suppressed by about 34% from 0.763 deg of the ISC to 0.506 deg. Thus, the iISC was utilized for the hybrid analysis of the FLC and the SMC.

Furthermore, the response of the FLC, SMC, iISC+FLC, and the iISC+SMC is analyzed.As shown in Fig.9a, the effect of adding the ISC can be seen to slow down the rise time for the FLC.However, both the iISC+FLC and the FLC reached the settling time as specified. Interestingly, the r.m.s of the tip deflection of FLC was significantly suppressed by about 64% after adding the iISC from 0.9244 to 0.3281deg, as shown in Fig.9b.On the other hand, Fig.9c shows the response of the SMC and the iISC+SMC.However, adding the ISC did not show much reduced rise time because as the SMC is model dependent, the ISC affected its response.Thus, to have reasonable comparison with other controllers, the SMC was re-tune with different parameters.Still, after achieving the desired settling time for good position tracking, the r.m.s of the SMC was greatly suppressed from 1.6536 deg to 0.2445 deg, representing 85% of tip deflection reduction as shown in Fig.9d.

B. SENSITIVITY ANALYSIS TO SYSTEM PARAMETER VARIATIONS

The discussion in the previous section showed that the iISC, FLC and SMC algorithms improve the automation of the control performance of the FLM system.Nevertheless, the analysis was performed using the exact values of the parameters.To study the sensitivity of the controllers to changes of system's parameters, the impact of the key parameters, namely the link's stiffness, mass and length, were studied.In each case, the value of the parameters were increased by 25% and then decreased by the same amount.The comparison is made in relation to the design parameters (exact). The higher the deviation of the response from the exact response the higher the sensitivity of the controller to parameter variations.This will allow to study the sensitivity of the controllers to modelling errors.The optimal control will be less sensitive to those changes.

1) INFLUENCE OF VARYING LINK MASS (m_l)

The automation of the FLM can be affected by changes in the link's mass. Therefore, it is important to evaluate the robustness of the controllers to such variations. The impact of varying the link's mass is illustrated in Fig. 10. The system retained good tracking of the desired position whereby the system settled effectively without any overshoot for the iISC+FLC (Fig. 10a), whereas the settling time for the iISC+SMC were affected slightly with an under-shoot of 0.8% (29.77 deg) as shown in Fig. 10b.

Similarly, the maximum velocity of iISC+SMC was within the range 80±1.7deg/s as compared to the iISC+FLC with 94±1.6 deg/s, as shown in Fig. 10(c-d). The response pattern remains largely the same for the mass changes in relation to the tip deflection of the FLM, with maximum tip deflection of 1.6±0.23 deg, and1.0±0.16deg, respectively for the iISC+FLC, and iISC+SMC, as shown in Fig. 10(e-f).

2) INFLUENCE OF VARYING LINK LENGTH (L_l)

The automation and control of the FLM are significantly affected by the length of the link.Thus, it is crucial to evaluate how this parameter impacts the controllers' performance.This study examined the effects of altering the length of the FLM's link on the performance of the position tracking, velocity, and tip deflection control, respectively.Figure 11 shows the responses of length variation for the iISC+FLC, and iISC+SMC.The controllers maintained good position tracking with both reaching the settling time of 1 second.However, zooming-in for the iISC+SMC shows that the SMC's performance can be affected as compared to that of the iISC+FLC.Although very small, it can be observed that increasing the length resulted in an increased in system velocity, and tip deflection, respectively for the two hybrid controllers.The maximum velocity was within 94±0.5deg/s, and 79±0.6deg/s for the iISC+FLC and iISC+SMC, respectively, as shown in Fig.11(c-d). Also, the maximum tip deflection was not much affected by the changes of link length as shown in Fig.11(e-f).

3) INFLUENCE OF VARYING LINK STIFFNESS (k_l)

As the FLM moves, its deflection depends on the flexibility of the link.The flexibility is in turn proportional to the stiffness of the link. Figure 12 illustrates the impact of stiffness change on the control system.The system retained good tracking of the desired position whereby the system settled effectively without any overshoot for the iISC+FLC (Fig.12a), whereas the settling time for the iISC+SMC were affected slightly with an overshoot of 1.9% (30.19 deg), and undershoot of 4.3% (29.57 deg) as shown in Fig.12b.Similarly, the maximum velocity of iISC+FLC, and iISC+SMC for the increased and decreased mass of the link were within 94±0.52deg/s, and 80±2.65deg/s, respectively.The response pattern of the tip deflection of the FLM shows that the tip deflection decreases with the increasing stiffness with the maximum deflection of 1.6±0.4deg, and 1.0±0.31 deg for the iISC+FLC, and iISC+SMC, respectively, as shown in Fig.12(e-f).

C. DISCUSSION

In the previous sections, three different controllers were analyzed for the possible application of precise automation of the rotary FLM.The effect of model error was analyzed by deliberately changing the parameters of the FLM.The summary of the analysis for the five performance criteria, namely, maximum velocity of the link, maximum tip deflection, r.m.s of the deflection, percentage overshoot, and settling time of the link were considered.

1) TIME RESPONSE SPECIFICATIONS

To analyze the performance of the control system, the time response performance indicators namely, rise time (T_r),

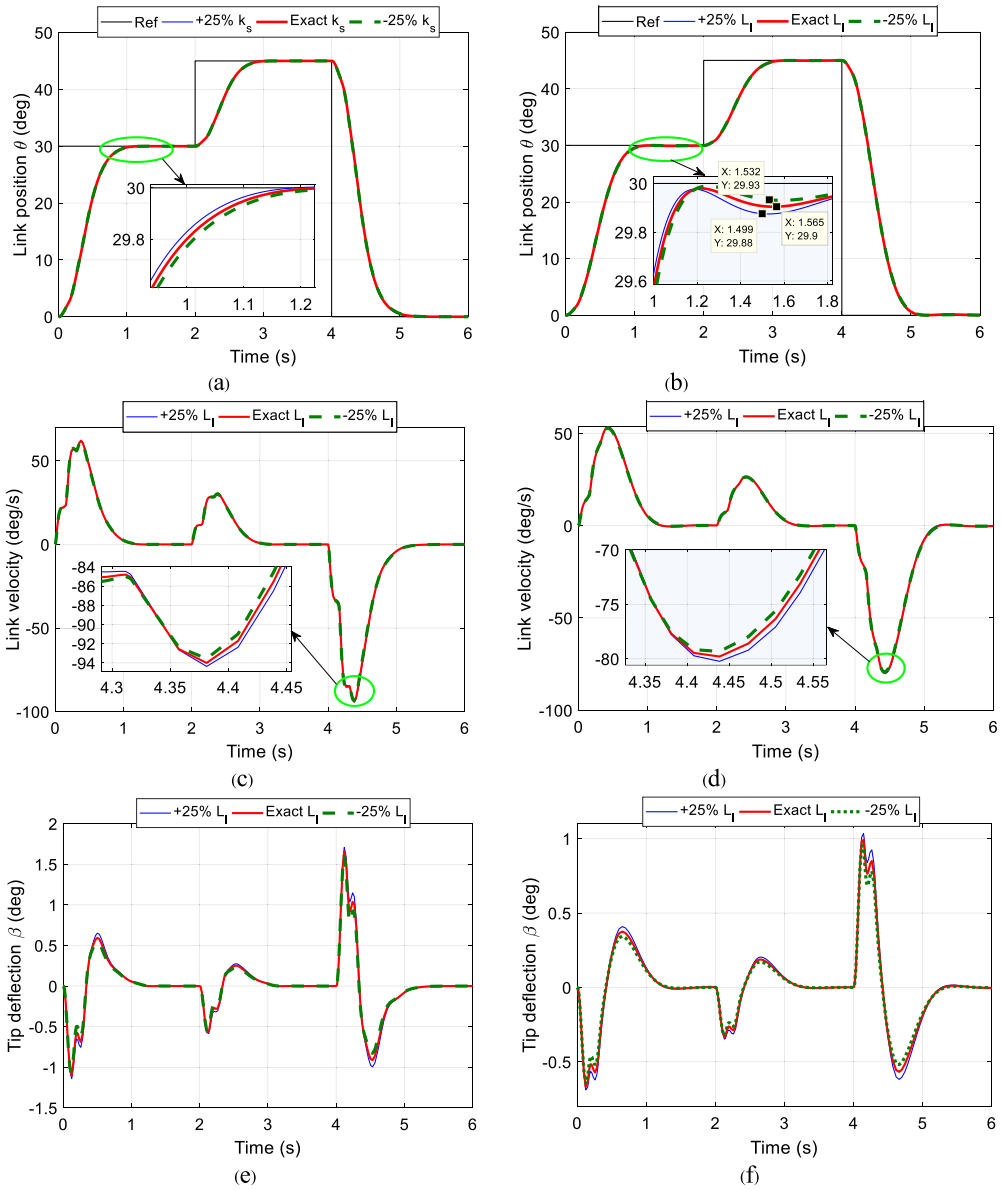

FIGURE 11. Sensitivity to changes of link length: (a) Position control of iISC+FLC; (b) Position tracking of iISC+SMC; (c) Link velocity for iISC+FLC; (d) Link velocity for iISC+SMC; (e) Tip deflection for iISC+FLC; (f) Tip deflection for iISC+SMC.

TABLE 4. Time response specifications for iISC+FLC, and iISC+SMC.

Parameter	Cases	Rise Time, T_r [S]		Percentage Overshoot, OS [%]		Settling Time, T_s [S]		Max. Settling [deg]	
		iISC+FLC	iISC+SMC	iISC+FLC	iISC+SMC	iISC+FLC	iISC+SMC	iISC+FLC	iISC+SMC
Stiffness (k_l)	+25%	0.5195	0.5800	0.0000	0.7084	0.8964	0.9654	30.0010	30.1925
	Exact	0.5197	0.5711	0.0000	0.0218	0.8962	0.9675	30.0004	29.9776
	-25%	0.5190	0.5570	0.0000	0.0000	0.8988	0.9882	30.0005	29.9736
Mass (m_l)	+25%	0.5020	0.5520	0.0738	0.1775	0.8622	0.9231	30.0226	30.0191
	Exact	0.5190	0.5706	0.0000	0.0224	0.8954	0.9667	30.0004	29.9779
	-25%	0.5351	0.5925	0.0000	0.1693	0.9261	1.0038	30.0003	30.0383
Length(L_l)	+25%	0.5135	0.5659	0.0100	0.0188	0.8877	0.9560	30.0034	29.9742
	Exact	0.5181	0.5709	0.0000	0.0214	0.8955	0.9665	30.0004	29.9776
	-25%	0.5225	0.5760	0.0000	0.0438	0.9031	0.9766	30.0004	29.9876

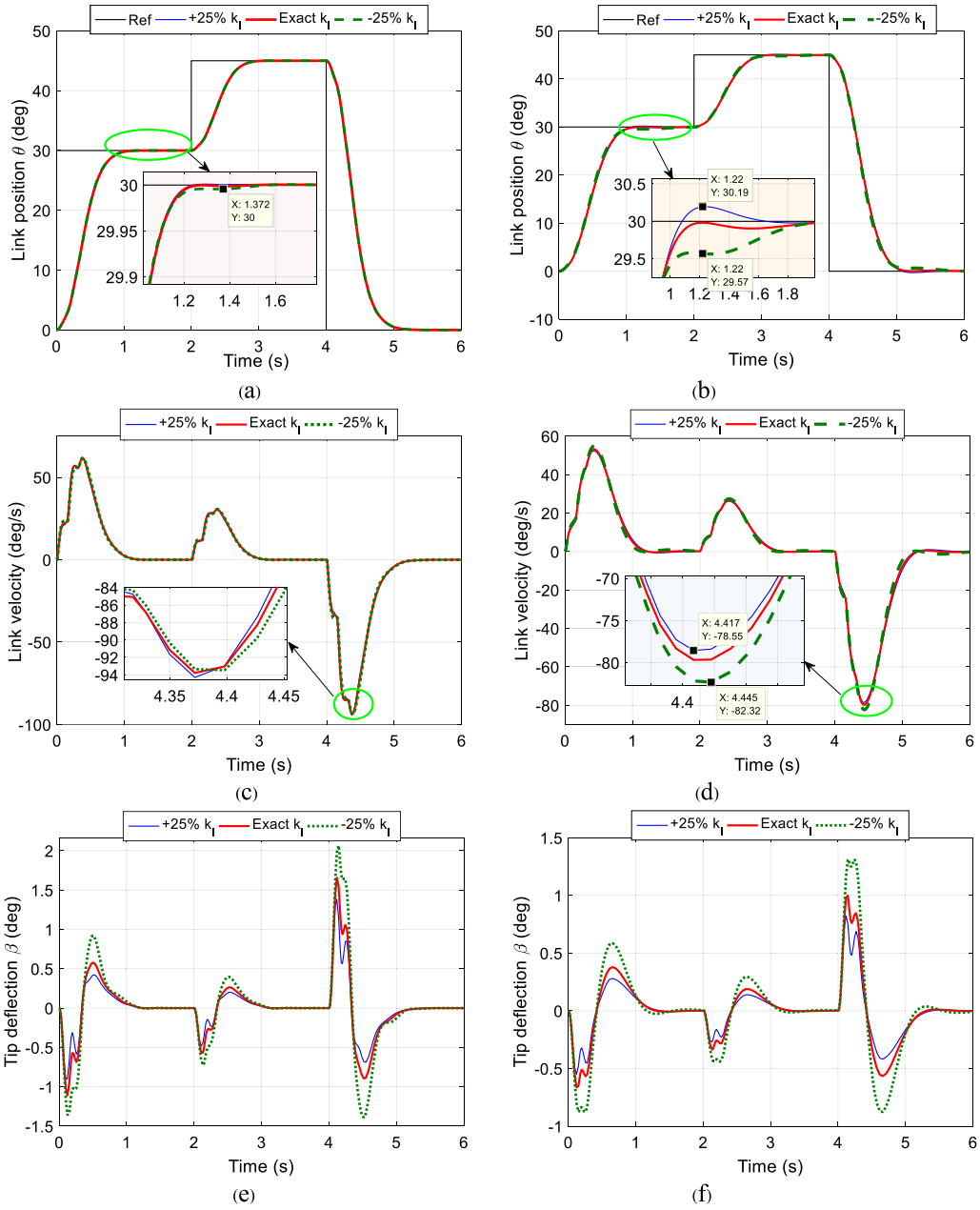

FIGURE 12. Sensitivity to changes of link stiffness: (a) Position tracking of iISC+FLC; (b) Position tracking of iISC+SMC; (c) Link velocity for iISC+FLC; (d) Link velocity for iISC+SMC; (e) Tip deflection for iISC+FLC; (f) Tip deflection for iISC+SMC.

percentage overshoot (OS), and settling time (T_s) of the link were considered. These parameters provide adequate performance comparison of the controllers. Table 4 shows the time response specification for the three control cases. Here, the default settling time within 2% of the final value is considered. For the T_r which shows how quick the control respond to the input signal, the average is 0.52 s and 0.56 s for the iISC+FLC, and iISC+SMC, respectively. For the OS, the controllers demonstrated good tracking with virtually zero overshot for the iISC+FCL, and significantly small OS of less 1% for the iISC+SMC. In addition, the final settlement of the system was reached at approximately 0.9 s and 1 s for the iISC+FLC, and iISC+SMC which reaffirms that the iISC+FLC settled faster. The graphical representation of the T_s for the three cases were further analyzed in Fig.13. It demonstrated the effect of changing the robot parameters to the settling time.

2) SENSITIVITY ANALYSIS

It is worth noting that although the iISC suppressed the oscillation very well, it does not provide position control in a standalone configuration.Therefore, it was hybridized

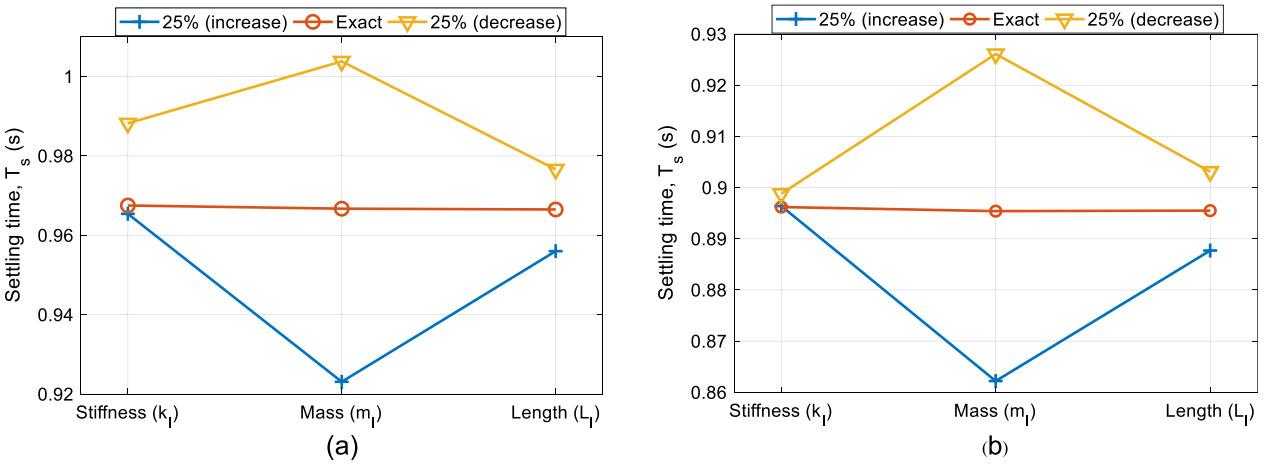

FIGURE 13. Settling time for the three cases: (a) iISC+SMC; (b) iISC+FLC. In each case, changing the mass has more effect to the settlement as compared to other parameters.

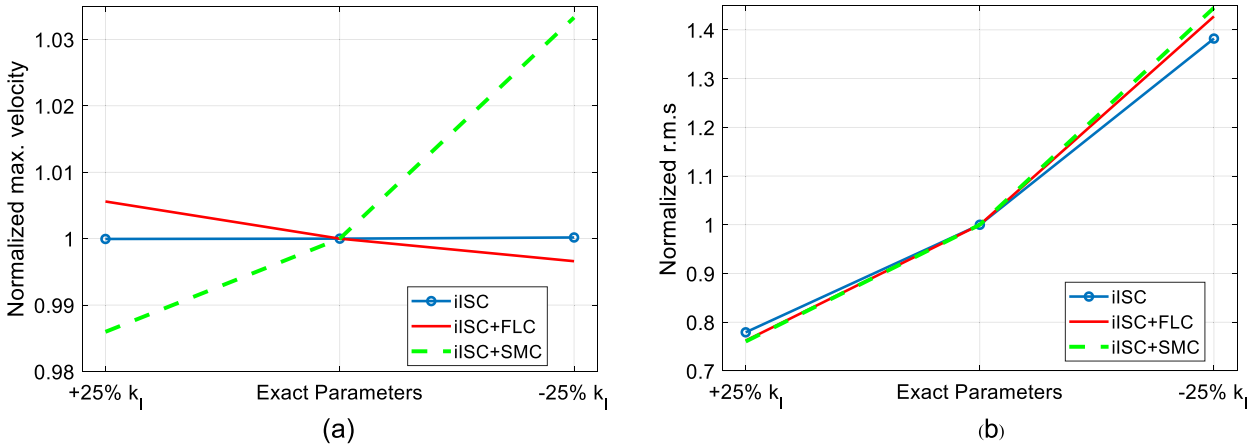

FIGURE 14. Normalized sensitivity analysis of iISC, iISC+FLC, and iISC+SMC to changes of FLM stiffness. Deviation from one shows the sensitivity of controllers to parameter change: (a) Max. velocity; (b) R.M.S.

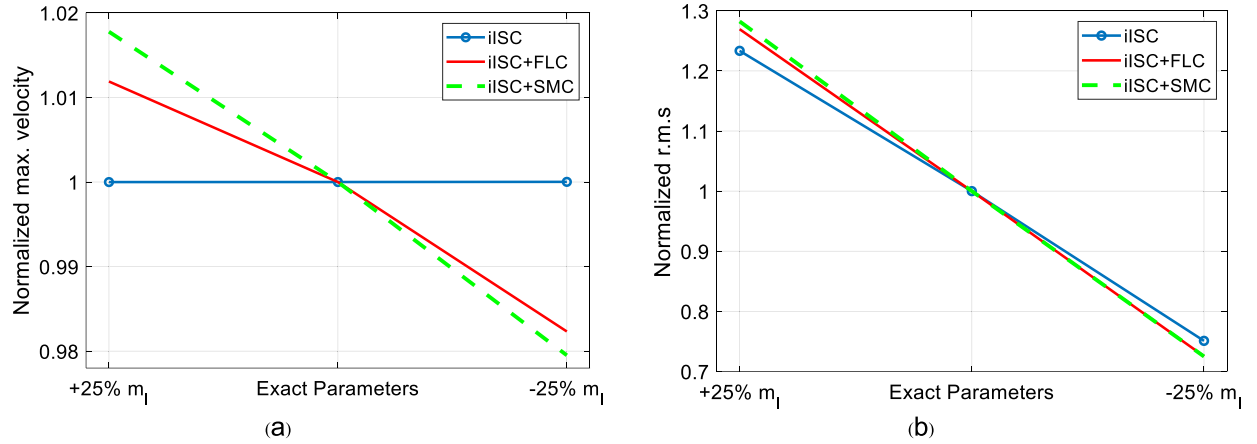

FIGURE 15. Normalized sensitivity analysis of iISC, iISC+FLC, and iISC+SMC to changes of FLM mass. Deviation from one shows the sensitivity of controllers to parameter change: (a) Max. velocity; (b) R.M.S.

with the two controller to assess their performance for both the position and the deflection control.As shown in Table 5, the iISC+FLC had faster response which leads to a bit higher angular oscillation as compared to the iISC+SMC.To

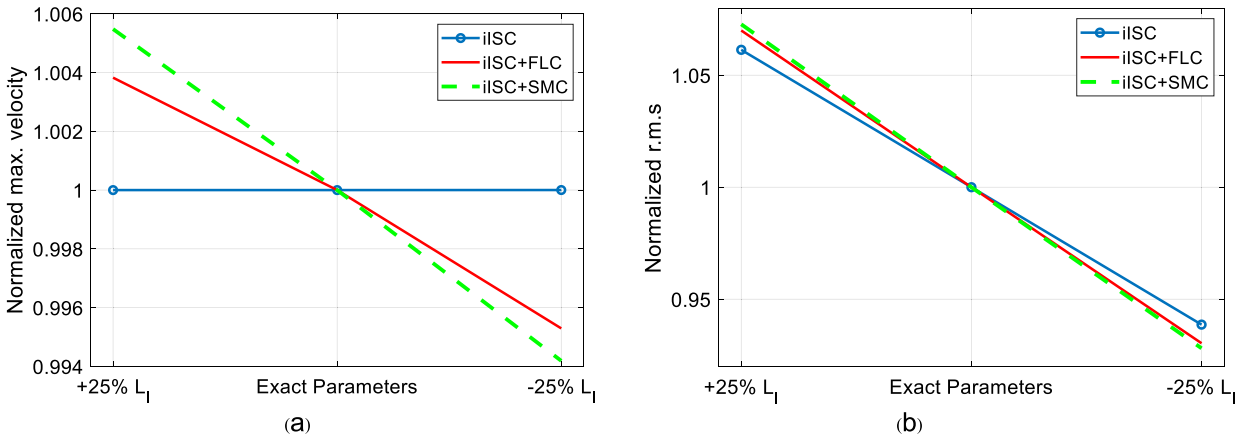

FIGURE 16. Normalized sensitivity analysis of iISC, iISC+FLC, and iISC+SMC to changes of FLM length. Deviation from one shows the sensitivity of controllers to parameter change: (a) Max. velocity; (b) R.M.S.

TABLE 5. Sensitivity analysis for iISC+FLC, and iISC+SMC.

Parameter	Cases	Max. velocity [m/s]		Max. tip deflection [deg]		R.M.S [deg]	
		iISC+FLC	iISC+SMC	iISC+FLC	iISC+SMC	iISC+FLC	iISC+SMC
Stiffness (k_l)	+25%	94.3056	78.5504	1.3828	0.8218	0.2545	0.1859
	Exact	93.7807	79.6681	1.6558	0.9987	0.3339	0.2445
	-25%	93.4623	82.3211	2.0645	1.3120	0.4767	0.3534
Mass (m_l)	+25%	94.9570	81.3265	1.8154	1.1643	0.4321	0.3175
	Exact	93.8414	79.9063	1.6593	0.9950	0.3404	0.2476
	-25%	92.1828	78.2689	1.4207	0.8510	0.2469	0.1795
Length(L_l)	+25%	94.3621	80.2307	1.7063	1.0353	0.3410	0.2581
	Exact	94.0024	79.7934	1.6607	0.9907	0.3187	0.2406
	-25%	93.5598	79.3296	1.6101	0.9563	0.2965	0.2233

clearly analyze the sensitivity of the controllers, a normalized analysis of the controllers about the base values (exact) is conducted.With the unity (1) being the ideal values, deviation from this value shows how sensitive a specific controller is to variation of the parameters.Figure 14a-b shows the sensitivity of the controllers to changes of stiffness.For the normalized maximum velocity, the iISC maintain a constant velocity while the iISC+FLC deviate by 0.0056 as compared to the iISC+SMC with 0.033, as shown in Fig.14a.In all cases, the sensitivity of the maximum velocities of the controllers is not much affected.

Similarly, the deviation of the normalized r.m.s (Fig.14b) shows that increasing the flexibility (decreasing stiffness) affects the tip deflection by about 0.427, and 0.446, for the iISC+FLC, and iISC+SMC, respectively.On the other hand, increasing or decreasing the link mass (Fig.15a-b) or length (Fig.16a-b) shows similar pattern, though, changing the link length has the smallest sensitivity.For all the analyses, the iISC+FLC shows better sensitivity response as compared to iISC+SMC.

V. CONCLUSION

The ever-increasing demand of improved productivity in the manufacturing sector encourage the research and development of robotic flexible manipulators that are generally cost-effective, and possessed high degree of maneuverability as compared to the rigid manipulators. The main objective of this study is to achieve precise automation of a rotary FLM in terms of link position tracking, and tip deflection suppression, which are often challenging for the FLM. The paper presents the possible hybridization of iISC with a single state feedback FLC, and SMC. The results of the control under different scenarios were obtained and analyzed. The summary of the whole paper can be drawn as follows:

(1) An improved input shaper (iISC) which reduces the excessive delay and chattering of the traditional ISC was designed. Apart from increasing the response time of the ISC, the iISC also improved the tip deflection suppression by at least 34%. Though proved to be an effective tip deflection suppression technique, the iISC cannot provide position tracking.

(2) The iISC was hybridized with the non-model based FLC (iISC+FLC), and a model-based SMC (iISC+SMC) for both position, and deflection suppression. Only the feedback of one state (position) was utilized for the closed-loop schemes. By analyzing the maximum velocity of the FLM, the constant velocity of the iISC (53 deg/s) was improved by

about 77% (94 deg/s) and 51% (80 deg/s) for the iISC+FLC, and iISC+SMC, respectively.

(3) By using the r.m.s as the performance index for the tip deflection analysis, the oscillation suppression of the FLC (0.92 deg), and SMC (1.65 deg) was improved by about 64% (0.33 deg) and 85% (0.24 deg) for the iISC+FLC, and iISC+SMC, respectively. Nonetheless, there was little delay penalty for adding the iISC to the hybrid system.

(4) The sensitivity analysis to variations in system parameters was conducted. The results demonstrated that the controllers are more sensitive to changes of link stiffness while more robust to changes of link length. The normalized r.m.s analysis shows that in addition to using only one single state feedback, the iISC+FLC has better performance as compared to the iISC+SMC. The future work will focus the real-time experimental validation of the dynamic analysis on the physical system.

ACKNOWLEDGMENT

Special thanks is given to CU VISION X for supporting the hardware and software used in this research and to the Ignite Innovation Laboratory for supporting the research innovation eco-system used.

REFERENCES

[1] S. A. Kumar, R. Chand, R. P. Chand, and B. Sharma, "Linear manipulator: Motion control of an n-link robotic arm mounted on a mobile slider," *Heliyon*, vol. 9, no. 1, Jan. 2023, Art. no. e12867, doi: 10.1016/j.heliyon.2023.e12867.

[2] M. Uyar, "Comparison of classical and newly designed motion profiles for motion-based control of flexible composite manipulator," *J. Brazilian Soc. Mech. Sci. Eng.*, vol. 44, no. 9, pp. 1–18, Sep. 2022, doi: 10.1007/s40430-022-03725-2.

[3] E. Skosarev and S. Kolyubin, "Case study on energy-aware position control for flexible link mechatronic systems," in *Proc. IEEE Int. Conf. Mechatronics (ICM)*, vol. 1, no. 8, Mar. 2019, pp. 617–621.

[4] P. Ma, R. Xia, X. Wang, X. Zhang, G. Królczyk, P. Gardoni, and Z. Li, "An active control method for vibration reduction of a single-link flexible manipulator," *J. Low Freq. Noise, Vib. Act. Control*, vol. 41, no. 4, pp. 1497–1506, Dec. 2022, doi: 10.1177/14613484221094982.

[5] M. I. Solihin, L. W. Hong, C. K. Ang, M. Rizon, and A. Radwan, "Robust H∞ controller design for flexible link manipulator based on constrained metaheuristics optimization algorithms," in *Proc. Int. Artif. Life Robot.*, 2020, pp. 338–342, doi: 10.5954/icarob.2020.os10-5.

[6] G. Van de Perre, T. Hubert, T. Verstraten, and B. Vanderborght, "Investigating the potential of flexible links for increased payload to mass ratios for collaborative robotics," *IEEE Access*, vol. 11, pp. 15981–15995, 2023, doi: 10.1109/ACCESS.2023.3244402.

[7] M. Shi, B. Rong, J. Liang, W. Zhao, and H. Pan, "Dynamics analysis and vibration suppression of a spatial rigid-flexible link manipulator based on transfer matrix method of multibody system," *Nonlinear Dyn.*, vol. 111, no. 2, pp. 1139–1159, Jan. 2023, doi: 10.1007/s11071-022-07921-6.

[8] J. Shen, W. Zhang, S. Zhou, and X. Ye, "Fuzzy adaptive compensation control for space manipulator with joint flexibility and dead zone based on neural network," *Int. J. Aeronaut. Space Sci.*, vol. 24, no. 3, pp. 876–889, Jul. 2023, doi: 10.1007/s42405-023-00570-y.

[9] O. M. Omisore, S. Han, J. Xiong, H. Li, Z. Li, and L. Wang, "A review on flexible robotic systems for minimally invasive surgery," *IEEE Trans. Syst., Man, Cybern. Syst.*, vol. 52, no. 1, pp. 631–644, Jan. 2022, doi: 10.1109/TSMC.2020.3026174.

[10] H. Bilal, B. Yin, A. Kumar, M. Ali, J. Zhang, and J. Yao, "Jerk-bounded trajectory planning for rotary flexible joint manipulator: An experimental approach," *Soft Comput.*, vol. 27, no. 7, pp. 4029–4039, Apr. 2023, doi: 10.1007/s00500-023-07923-5.

[11] T. S. Lee and E. A. Alandoli, "A critical review of modelling methods for flexible and rigid link manipulators," *J. Brazilian Soc. Mech. Sci. Eng.*, vol. 42, no. 10, pp. 1–14, Oct. 2020, doi: 10.1007/s40430-020-02602-0.

[12] E. A. Alandoli and T. S. Lee, "A critical review of control techniques for flexible and rigid link manipulators," *Robotica*, vol. 38, no. 12, pp. 2239–2265, Dec. 2020, doi: 10.1017/S0263574720000223.

[13] M. Shao, Y. Huang, and V. V. Silberschmidt, "Intelligent manipulator with flexible link and joint: Modeling and vibration control," *Shock Vib.*, vol. 2020, pp. 1–15, Jan. 2020, doi: 10.1155/2020/4671358.

[14] B. Altıner, A. Delibaşı, and B. Erol, "Modeling and control of flexible link manipulators for unmodeled dynamics effect," *Proc. Inst. Mech. Eng., I, J. Syst. Control Eng.*, vol. 233, no. 3, pp. 245–263, Mar. 2019, doi: 10.1177/0959651818791071.

[15] M. Shi, Y. Cheng, B. Rong, W. Zhao, Z. Yao, and C. Yu, "Research on vibration suppression and trajectory tracking control strategy of a flexible link manipulator," *Appl. Math. Model.*, vol. 110, pp. 78–98, Oct. 2022, doi: 10.1016/j.apm.2022.05.030.

[16] H. Yang and J. Liu, "Active vibration control for a flexible-link manipulator with input constraint based on a disturbance observer," *Asian J. Control*, vol. 21, no. 2, pp. 847–855, Mar. 2019, doi: 10.1002/asjc.1793.

[17] R. Fareh, M. Al-Shabi, M. Bettayeb, and J. Ghommam, "Robust active disturbance rejection control for flexible link manipulator," *Robotica*, vol. 38, no. 1, pp. 118–135, Jan. 2020, doi: 10.1017/S026357471900050X.

[18] X. Cheng, H. Liu, and W. Lu, "Chattering-suppressed sliding mode control for flexible-joint robot manipulators," *Actuators*, vol. 10, no. 11, p. 288, Oct. 2021, doi: 10.3390/act10110288.

[19] J. Zhu, J. Zhang, J. Zhu, L. Zeng, and Y. Pi, "A composite controller for manipulator with flexible joint and link under uncertainties and disturbances," *J. Vib. Control*, vol. 28, nos. 9–10, pp. 1148–1164, May 2022, doi: 10.1177/1077546320988196.

[20] A. Belherazem and M. Chenafa, "Passivity based adaptive control of a single-link flexible manipulator," *Autom. Control Comput. Sci.*, vol. 55, no. 1, pp. 1–14, Jan. 2021, doi: 10.3103/S0146411621010028.

[21] H. Huang, G. Tang, H. Chen, L. Han, and D. Xie, "Dynamic modeling and vibration suppression for two-link underwater flexible manipulators," *IEEE Access*, vol. 10, pp. 40181–40196, 2022, doi: 10.1109/ACCESS.2022.3164706.

[22] M. Akdağ and H. Şen, "Investigation of performance and sensitivity of S-curve motion profiles on reduction in flexible manipulator vibrations," *Arabian J. Sci. Eng.*, pp. 1–14, Feb. 2023, doi: 10.1007/s13369-023-07639-6.

[23] L. Li, F. Cao, and J. Liu, "Adaptive vibration control for constrained moving vehicle-mounted nonlinear 3D rigid-flexible manipulator system subject to actuator failures," *J. Vib. Control*, Jul. 2022, Art. no. 107754632211132, doi: 10.1177/10775463221113222.

[24] X. Ye, J. Dong, W. Wang, J. Lu, and J. Wang, "Design and performance analysis of magnetorheological grease flexible manipulator gripper," *J. Mech. Sci. Technol.*, vol. 37, no. 3, pp. 1–12, Feb. 2023, doi: 10.1007/s12206-023-0212-4.

[25] W. Yao, Y. Guo, Y.-F. Wu, and J. Guo, "Robust adaptive dynamic surface control of multi-link flexible joint manipulator with input saturation," *Int. J. Control, Autom. Syst.*, vol. 20, no. 2, pp. 577–588, Feb. 2022, doi: 10.1007/s12555-020-0176-x.

[26] B. Guo, P. Wang, Z. Zhao, S. Duan, and H. Lei, "Design and experiments of an origami-inspired pneumatic flexible manipulator," *Acta Mechanica Solida Sinica*, vol. 36, pp. 1–8, Jan. 2023, doi: 10.1007/s10338-022-00376-7.

[27] G. Bastos, "A non-inherent parametric estimation for dynamical equivalence of flexible manipulators," *Optim. Control Appl. Methods*, vol. 43, no. 3, pp. 825–841, May 2022, doi: 10.1002/oca.2853.

[28] F. A. Lara-Molina and R. S. Gonçalves, "Reliability-based optimization of flexible manipulators," *J. Vib. Eng. Technol.*, pp. 1–16, Oct. 2022, doi: 10.1007/s42417-022-00737-z.

[29] Quanser Inc. *Rotary Flexible Link*. Accessed: May 5, 2023. [Online]. Available: https://www.quanser.com/products/rotary-flexible-link/

[30] A. Alhassan, Z. Mohamed, A. M. Abdullahi, A. A. Bature, A. Haruna, and N. M. Tahir, "Input shaping techniques for sway control of a rotary crane system," *J. Teknol.*, vol. 80, no. 1, pp. 61–69, 2018, doi: 10.11113/jt.v80.10297.

[31] Zulfatman, M. Marzuki, and N. A. Mardiyah, "Two-link flexible manipulator control using sliding mode control based linear matrix inequality," *IOP Conf. Ser., Mater. Sci. Eng.*, vol. 190, no. 1, Apr. 2017, Art. no. 012008, doi: 10.1088/1757-899X/190/1/012008.

[32] M. A. Shehu, A. J. Li, B. Huang, Y. Wang, and B. Liu, "Comparative analysis of neural-network and fuzzy auto-tuning sliding mode controls for overhead cranes under payload and cable variations," *J. Control Sci. Eng.*, vol. 2019, pp. 1–14, Jan. 2019, doi: 10.1155/2019/1480732.
[33] C.-W. Ha, D. Lee, K.-H. Rew, and K.-S. Kim, "An impulse-time perturbation approach for a symmetric extra-insensitive input shaper," *Int. J. Control, Autom. Syst.*, vol. 16, no. 3, pp. 1239–1246, Jun. 2018, doi: 10.1007/s12555-017-0045-y.
[34] M. Shirzadeh, A. Amirkhani, N. Tork, and H. Taghavifar, "Trajectory tracking of a quadrotor using a robust adaptive type-2 fuzzy neural controller optimized by cuckoo algorithm," *ISA Trans.*, vol. 114, pp. 171–190, Aug. 2021, doi: 10.1016/j.isatra.2020.12.047.
[35] K. Adamiak and A. Bartoszewicz, "Novel power-rate reaching law for quasi-sliding mode control," *Energies*, vol. 15, no. 15, pp. 1–14, 2022, doi: 10.3390/en15155446.
[36] K. B. Devika and S. Thomas, "Power rate exponential reaching law for enhanced performance of sliding mode control," *Int. J. Control, Autom. Syst.*, vol. 15, no. 6, pp. 2636–2645, Dec. 2017, doi: 10.1007/s12555-016-0736-9.
[37] F. Xu, N. An, J. Mao, and S. Yang, "A new variable exponential power reaching law of complementary terminal sliding mode control," *Complexity*, vol. 2020, pp. 1–11, Oct. 2020, doi: 10.1155/2020/8874813.

AHMAD BALA ALHASSAN received the B.Eng. degree in electrical engineering from Bayero University, Kano (BUK), Nigeria, in 2012, the M.Eng. degree in mechatronics and automatic control from the University of Technology Malaysia (UTM), in 2016, and the Ph.D. degree in mechanical engineering from Xi'an Jiaotong University (XJTU), China, in 2022.

He is currently a Postdoctoral Fellow with Chulalongkorn University, Thailand. He has authored and coauthored many research articles and international conference papers on dynamic analysis and control of overhead crane systems, inverted pendulum, rehabilitation robots, elderly-assistant robots, and power transmission line inspection robots. His current research interests include modeling, simulation, and control of mechatronics systems.

RATCHATIN CHANCHAROEN received the B.S. degree in mechanical engineering from Chulalongkorn University, Thailand, in 1991, the M.S. degree in mechanical engineering from Oregon State University, in 1994, and the Ph.D. degree in mechanical engineering from Chulalongkorn University, in 2000.

He is currently an Associate Professor with the Department of Mechanical Engineering, Chulalongkorn University. He is a principal investigator and a co-investigator of a number of research grants in robotics and the manager of a number of industrial projects in design and control. He has 20 years of experience in robotics research, including both manipulators and mobile robots, and ten years in teaching both robotics and mechatronics with the university level. During these years, he has designed and built more than 20 robots in various configurations and has published more than 20 research papers and one text book titled *Linear Control Systems* (in Thai). His major research activities involve tele-operation and control of robotics manipulators and mobile robots using various kinds of sensors, especially force and vision. His current research interests include the design of a telerobot, a new type of robot, to work closely with humans to do a higher level of tasks; and robotics and mechatronics, including new parallel robot configuration, new hardware processors, electronics, control algorithms, and intelligence. The telerobot is designed with a lighter frame, less power consumption, a small footprint controller, and a higher level of intelligence, compared to the industrial robot, to safely work in our working space. This type of robot will be populated in the near future as more complex tasks are demanded.

BASHIR BALA MUHAMMAD received the bachelor's degree in electrical engineering from Bayero University, Kano (BUK), Nigeria, in 2010, the master's degree in mechatronics and automatic control from the University of Technology Malaysia (UTM), in 2015, and the Ph.D. degree in mechanical engineering from Northwestern Polytechnical University (NWPU), Xi'an, China, in 2019. He spent two years in manufacturing industry (Dangote Industries Ltd.) as a Maintenance Engineer and three years as a Lecturer with the Air Force Institute of Technology, Kaduna. He is currently a Postdoctoral Fellow with Chulalongkorn University, Thailand. His current research interests include control theory and mechatronics engineering.

GRIDSADA PHANOMCHOENG received the B.S. degree from Chulalongkorn University, Bangkok, Thailand, in 2002, and the M.S. degree in aerospace engineering and mechanics and the Ph.D. degree in control science and dynamical systems from the University of Minnesota, Twin Cities, Minneapolis, MN, USA, in 2007 and 2011, respectively.

In 2012, he was a Postdoctoral Researcher with the Dr. Rajamani's Mechanical Engineering Laboratory, University of Minnesota, Twin Cities. He is currently a Faculty Member of mechanical engineering with Chulalongkorn University. His research interests include advanced control system design, observer design for nonlinear systems, system identification, applications to automotive systems, energy harvesting, and machine vision.